Tuning the Tricritical Point with Spin-Orbit Coupling in Polarized Fermionic Condensates

Renyuan Liao, Yu Yi-Xiang, and Wu-Ming Liu

National Laboratory for Condensed Matter Physics, Institute of Physics, Chinese Academy of Sciences, Beijing 100190, China

(Received 27 October 2011; published 22 February 2012)

We investigate a two-component atomic Fermi gas with population imbalance in the presence of Rashba-type spin-orbit coupling (SOC). As a competition between SOC and population imbalance, the finite-temperature phase diagram reveals a large variety of new features, including the expanding of the superfluid state regime and the shrinking of both the phase separation and the normal regimes. For sufficiently strong SOC, the phase separation region disappears, giving way to the superfluid state. We find that the tricritical point moves toward a regime of low temperature, high magnetic field, and high polarization as the SOC increases.

DOI: 10.1103/PhysRevLett.108.080406 PACS numbers: 05.30.Fk, 03.75.Hh, 03.75.Ss, 67.85.−d

The recent experimental realization of a synthetic gauge field [1] and spin-orbit coupling [2] opens a new arena to explore quantum many-body systems of ultracold atoms. The engineered spin-orbit coupling (SOC) (with equal Rashba and Dresselhaus strength) in a neutral atomic Bose-Einstein condensate was accomplished by dressing two atomic spin states with a pair of lasers. The interaction between a quantum particle's spin and its momentum is crucial for spin Hall effects [3] and topological insulators [4], which has captured a great deal of attention in the condensed matter community. The engineered SOC, equally applicable for bosons and fermions, allows for the realization of topological insulators and topologically nontrivial states [5,6] in fermionic neutral atom systems, engendering broad interest in the physics community.

In anticipation of immediate experimental relevance involving SOC in fermionic atoms such as ^{6}Li and ^{40}K [6], intense theoretical attention has been paid to the physics of the Bose-Einstein condensate-BCS crossover [7–11] and polarized Fermi gases [12–14] in the presence of SOC. The SOC has been predicted to lead to various new phenomena. In particular, for the two-body problem, it gives rise to a two-body bound state even on the BCS side ($a_s < 0$) of a resonance [7]. For the many-body physics at mean-field level, it enhances BCS pairing via the increased density of states at low energy and leads to anisotropic superfluids through mixing of the spin singlet and triplet components [7–10,15].

Polarized fermionic condensates have been the focus of both theoretical and experimental research over the past years [16]. Various possible asymmetric superfluid phases have been proposed: for example, anisotropic or inhomogeneous superfluid states with crystalline structure (Fulde-Ferrell-Larkin-Ovchinnikov) [17], deformed Fermi surfaces [18], a homogeneous gapless (breached pair) superfluid state [19], and phase separation into the normal Fermi gases and fully paired superfluid state [20]. One of the key questions to ask is how SOC reshapes our understanding of these exciting systems. So far, most of the theoretical studies [7–14] have focused mainly on zero temperature, leaving the physics at finite temperature, which is experimentally relevant, largely intact. In this Letter, we are trying to address this question by conducting the following studies: First, we map out the finite-temperature phase diagram at the BCS side where mean-field theory gives quantitatively reasonable results. By determining the behavior of the tricritical point as a function of SOC strength, we can completely characterize the topology of the phase diagram without recourse to an extensive numerical treatment [21,22]. Second, we examine the physics at unitarity, which is experimentally relevant and theoretically interesting. Specifically, we consider the effect of SOC on the "spin susceptibility" and the critical temperature. Finally, we investigate the fate of breached pairing states [19] under SOC through the correlation functions.

We consider three-dimensional homogeneous two-species polarized Fermi gases interacting via an attractive contact potential with an isotropic in-plane Rashba spin-orbit coupling, described by the following Hamiltonian,

$$H = \int d^3\mathbf{r} \sum_{\sigma=\uparrow,\downarrow} \psi_\sigma^\dagger(\mathbf{r})\left(\frac{\hat{\mathbf{P}}^2}{2m} - \mu_\sigma\right)\psi_\sigma(\mathbf{r}) - g\int d^3\mathbf{r}\,\psi_\uparrow^\dagger(\mathbf{r})\psi_\downarrow^\dagger(\mathbf{r})\psi_\downarrow(\mathbf{r})\psi_\uparrow(\mathbf{r}) + H_{\mathrm{SO}}. \quad (1)$$

Here, $H_{\mathrm{SO}} = \lambda\sum_{\mathbf{k}} k_\perp[e^{-i\varphi_{\mathbf{k}}}\psi_{\mathbf{k}\uparrow}^\dagger\psi_{\mathbf{k}\downarrow} + \mathrm{H.c.}]$, with the transverse momentum $\mathbf{k}_\perp = (k_x, k_y)$ and $\varphi_{\mathbf{k}} = \mathrm{Arg}(k_x + ik_y)$. The strength of spin-orbit coupling λ can be tuned by atom-laser interaction [2]. We define the chemical potential μ and the magnetic field h such that $\mu_\uparrow = \mu + h$ and $\mu_\downarrow = \mu - h$. The spin imbalance between the two species is denoted by the polarization $P = (n_\uparrow - n_\downarrow)/(n_\uparrow + n_\downarrow)$. We consider pairing between different hyperfine species of the same atom, so we restrict ourself to a single mass m. The interaction strength g is expressed in terms of the s-wave scattering length a_s by using the

prescription $\frac{m}{4\pi a_s} = -\frac{1}{g} + \frac{1}{V}\sum_{\mathbf{k}} \frac{1}{2\epsilon_{\mathbf{k}}}$, where V is the volume and $\epsilon_{\mathbf{k}} = \mathbf{k}^2/2m$ (for convenience, we set $\hbar = k_B = 1$). We also define the Fermi momentum by using $k_F = (3\pi^2 n)^{1/3}$, with total density $n = n_\uparrow + n_\downarrow$, so that the Fermi velocity is $v_F = k_F/m$. Throughout our calculation, we will keep n fixed.

Within the framework of the imaginary-time field integral, the partition function of the system is $Z = \int d[\bar{\psi}, \psi] \exp(-S[\bar{\psi}, \psi])$ with the action $S[\bar{\psi}, \psi] = \int d\tau [\sum_\sigma \bar{\psi}_\sigma \partial_\tau \psi_\sigma + H(\bar{\psi}, \psi)]$. Introducing a bosonic field $\Delta(\mathbf{r}, \tau)$, which is believed to encapsulate the relevant low-energy degrees of freedom, we perform a Hubbard-Stratonovich transformation, and then the action becomes $S = \int d\tau [\sum_{\mathbf{k}\sigma} (\epsilon_{\mathbf{k}} - \mu_\sigma) \bar{\psi}_{\mathbf{k}\sigma} \psi_{\mathbf{k}\sigma} + H_{\mathrm{SO}}] + \int d\tau d^3\mathbf{r} (\frac{|\Delta^2|}{g} - \bar{\psi}_\uparrow \bar{\psi}_\uparrow - \bar{\Delta} \psi_\downarrow \psi_\uparrow)$. To bring the action in a compact form, we define a four-dimensional vector $\bar{\Psi}_{\mathbf{k}} = (\bar{\psi}_{\mathbf{k}\uparrow} \bar{\psi}_{\mathbf{k}\uparrow} \psi_{-\mathbf{k}\uparrow} \psi_{-\mathbf{k}\downarrow})$. Then the action can be cast as $S = \int d\tau \sum_{\mathbf{k}} [\frac{1}{2} \bar{\Psi}_{\mathbf{k}} (-\mathcal{G}^{-1}) \Psi_{\mathbf{k}} + \xi_{\mathbf{k}}]$, with the inverse Green's function defined as

$$\mathcal{G}^{-1} = \begin{pmatrix} -\partial_\tau - \xi_{\mathbf{k}\uparrow} & -\lambda k_\perp e^{-i\varphi_{\mathbf{k}}} & 0 & \Delta \\ -\lambda k_\perp e^{i\varphi_{\mathbf{k}}} & -\partial_\tau - \xi_{\mathbf{k}\downarrow} & -\Delta & 0 \\ 0 & -\bar{\Delta} & -\partial_\tau + \xi_{\mathbf{k}\uparrow} & -\lambda k_\perp e^{i\varphi_{\mathbf{k}}} \\ \bar{\Delta} & 0 & -\lambda k_\perp e^{-i\varphi_{\mathbf{k}}} & -\partial_\tau + \xi_{\mathbf{k}\downarrow} \end{pmatrix},$$

with $\xi_{\mathbf{k}\uparrow} = \epsilon_{\mathbf{k}} - \mu + h$, $\xi_{\mathbf{k}\downarrow} = \epsilon_{\mathbf{k}} - \mu - h$, and $\xi_{\mathbf{k}} = \epsilon_{\mathbf{k}} - \mu$. Integrating out the fermionic degrees of freedom, we obtain the effective action

$$S_{\mathrm{eff}} = \int d\tau d^3\mathbf{r} \frac{|\Delta|^2}{g} - \frac{1}{2} \mathrm{Tr} \ln(-\mathcal{G}^{-1}) + \beta \sum_{\mathbf{k}} \xi_{\mathbf{k}}. \quad (2)$$

Setting $\Delta = \Delta_0 + \delta\Delta$ and $\mathcal{G}_0^{-1} = \mathcal{G}^{-1}|_{\Delta=\Delta_0}$, we can write $\mathcal{G}^{-1} = \mathcal{G}_0^{-1} + \Sigma$. Expanding the effective action to the second order in the fluctuation Σ, we approximate the effective action to be $S_{\mathrm{eff}} \approx S_0 + S_g$, with $S_0 = \beta V \frac{|\Delta_0|^2}{g} + \sum_{\mathbf{k}s=\pm} [\frac{\beta}{2}(\xi_{\mathbf{k}} - E_{\mathbf{k}s}) - \ln(1 + e^{-\beta E_{\mathbf{k}s}})]$, $S_g = \beta V \sum_q \frac{\delta\bar{\Delta}(-q)\delta\Delta(q)}{g} + \frac{1}{4} \mathrm{Tr}[\mathcal{G}_0(k)\Sigma(-q)\mathcal{G}_0(k-q)\Sigma(q)] \equiv \beta V \sum_q \Gamma^{-1}(q)\bar{\Delta}(-q)\delta\Delta(q)$, where $k = (\mathbf{k}, iw_n)$, $q = (\mathbf{q}, i\nu_n)$, and the quasiparticle excitation spectrum $E_{\mathbf{k}\pm}$ determined by $E_{\mathbf{k}\pm}^2 = \xi_{\mathbf{k}}^2 + \Delta_0^2 + h^2 + \lambda^2 k_\perp^2 \pm 2\sqrt{\xi_{\mathbf{k}}^2 h^2 + \xi_{\mathbf{k}}^2 \lambda^2 k_\perp^2 + h^2 \Delta_0^2}$. While $E_{\mathbf{k}+}$ is always gapped, $E_{\mathbf{k}-}$ accommodates gapless excitations distributed symmetrically along $k_z = 0$ axis at $k_\perp = 0$: (i) For $\mu \geq \sqrt{h^2 - \Delta_0^2}$, it has four gapless excitation points at $k_z = \pm\sqrt{\mu \pm \sqrt{h^2 - \Delta_0^2}}$; (ii) for $\mu < \sqrt{h^2 - \Delta_0^2}$, it has only two gapless excitation points at $k_z = \pm\sqrt{\mu - \sqrt{h^2 - \Delta_0^2}}$.

Peculiar properties of the excitation spectrum are illustrated in Fig. 1, where the isoenergy surface for $E_{\mathbf{k}\pm} = 0.8E_F$ at unitarity ($1/k_F a_s = 0$) is shown at zero temperature. The red dashed curve is for $E_{\mathbf{k}-}$, the blue solid curve is for $E_{\mathbf{k}+}$, and the green dash-dotted circle is for a spherical isoenergy surface. The isoenergy surface is symmetric with respect to $k_z = 0$ and possesses rotation symmetry along the z axis. For balanced superfluid ($h = 0$), $E_{\mathbf{k}\pm} = \sqrt{(|\xi_{\mathbf{k}}| \pm \lambda k_\perp)^2 + \Delta_0^2}$, as depicted in Figs. 1(a) and 1(b), with $\lambda = 0.125 v_F$ and $\lambda = 0.25 v_F$, respectively. The anisotropy of the isoenergy surface increases as one increases the strength of SOC λ. It is interesting to notice that there exist two branches of isoenergy for both $E_{\mathbf{k}+}$ and $E_{\mathbf{k}-}$, due to the positiveness of the chemical potential in this case. This will lead to the enhancement of BCS pairing through increasing the density of states around the Fermi surface. $E_{\mathbf{k}+}$ and $E_{\mathbf{k}-}$ merge at $k_\perp = 0$ at which point the effects of SOC vanish. For $h = 0.1E_F$, the isoenergy surface is shown in Figs. 1(c) and 1(d), with $\lambda = 0.125 v_F$ and $\lambda = 0.25 v_F$, respectively. Here we have only one branch for both $E_{\mathbf{k}+}$ and $E_{\mathbf{k}-}$.

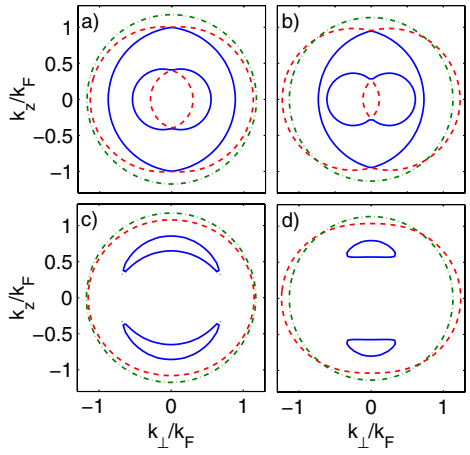

FIG. 1 (color online). Isoenergy surface ($E_{\mathbf{k}\pm} = 0.8E_F$) for the quasiparticle excitation spectrum at unitarity where $1/k_F a_s = 0$ at $T = 0$: (a) $h = 0$, $\lambda = 0.125 v_F$; (b) $h = 0$, $\lambda = 0.25 v_F$; (c) $h = 0.1E_F$, $\lambda = 0.125 v_F$; (d) $h = 0.1E_F$, $\lambda = 0.25 v_F$. The red dashed line is plotted for $E_{\mathbf{k}-}$, the blue solid line is for $E_{\mathbf{k}+}$, and the green dash-dotted circle is for a spherical isoenergy surface, plotted for comparison.

Interestingly, the curve for $E_{\mathbf{k}+}$ develops a lunar structure for low λ, as shown in Fig. 1(c), and increasing λ makes it blunt. For $E_{\mathbf{k}+}$ and $E_{\mathbf{k}-}$, the magnetic field h affects the isoenergy curve in the k_z direction: $E_{\mathbf{k}+}$ shrinks as h increases, while $E_{\mathbf{k}-}$ expands. The effect of SOC for $E_{\mathbf{k}+}$ and $E_{\mathbf{k}-}$ is opposite in the momentum space: The isoenergy curve in $k_\perp$ expands for $E_{\mathbf{k}-}$, while for $E_{\mathbf{k}+}$ it shrinks. The anisotropy nature of the excitation spectrum could be probed by momentum-resolved photoemission spectroscopy [23].

The phase diagram at finite temperature plays a key role in characterizing polarized fermionic condensates [21,24]. For a fixed interaction strength $1/k_F a_s$ and a fixed SOC strength λ, the phase diagram could be determined by the plane spanned by the temperature $T = 1/\beta$ and the magnetic field h. At sufficient low polarization or the magnetic field h, we expect a finite-temperature phase transition at which the superfluid order parameter vanishes continuously. Conversely, at low temperature, superfluidity is destroyed in a first-order fashion with increasing h. Across this phase transition at fixed h, the polarization jumps discontinuously. To determine the position of the phase boundaries, we must minimize the mean-field grand potential $\Omega_0 = S_0/\beta$ with respect to the BCS order parameter Δ_0. Such a mean-field analysis should provide a qualitative reasonable description at the weak-coupling BCS regime. In the absence of SOC ($\lambda = 0$), it is well known that there exists a finite-temperature tricritical point in the BCS limit, which is a natural consequence of having a first-order transition from the superfluid phase (SF) to the normal phase (N) at $T = 0$ and a second-order transition at zero polarization. First investigated by Sarma [25] in the context of superconductivity in the presence of a magnetic field h, the BCS tricritical is located at $(T_{\mathrm{crit}}/\Delta_0, h_{\mathrm{crit}}/\Delta_0) = (0.3188, 0.6061)$ [26], where $\Delta_0 = 8/e^2 E_F \exp(-\pi/2|k_F a_s|)$. The phase diagram spanned by T and h at $1/k_F a_s = -1$ for various SOC strengths is shown in the upper panel of Fig. 2. It consists of four different phases: the superfluid state with zero polarization (SF), the magnetized superfluid state with a finite polarization (SF_M), the normal state (N), and the phase separation (PS) regime enclosed by the first-order line and the second-order line. As the strength of SOC λ increases, the area of the phase separation region diminishes and eventually disappears for sufficiently large λ. With the increasing of SOC, the regime of SF diminishes very sharply, giving way to SF_M. This could be understood as follows: In the absence of SOC, the superfluid phase with balanced population is robust against the magnetic field h; in the presence of SOC, coupling between spin-up and spin-down components renders that the system is easily polarized, yielding the diminished region of SF. As a result of competition between SOC and the magnetic field, the phase space for SF_M expands as it allows a broadened range of the magnetic field. The intersection of the second-order line and the first-order line gives the position of the tricritical point, denoted as TP in Fig. 2. The evolution of the tricritical point is shown in the lower panel. As λ increases, T_{tri} decreases, while h_{tri} increases.

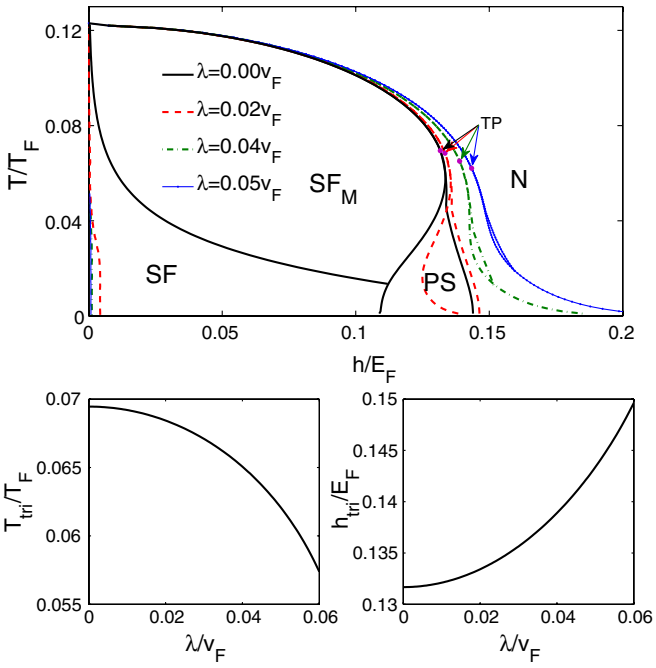

FIG. 2 (color online). Upper panel: Finite-temperature phase diagram as a function of T and h at $1/k_F a_s = -1$ (BCS side). There are four different phases: the N state, the PS state, the SF state, and the magnetized superfluid (SF_M). Above the tricritical point, the transition line separating the broken-symmetry state (SF_M) and the symmetric state (N) is of second order. Below the tricritical point (TP), it changes to the first order. Lower panel: The evolution of the tricritical point $(T_{\mathrm{tri}}/T_F, h_{\mathrm{tri}}/E_F)$ as a function of SOC strength λ.

The finite-temperature phase diagram for $1/k_F a_s = -1$ spanned by T and P is shown in Fig. 3. The $(T/T_F, P)$ phase diagram is highly reminiscent of the ^{3}He-^{4}He system, with P playing the role of the fraction of ^{3}He. This is not surprising, as the finite P system corresponds in general to a mixture of bosonic pairs and fermionic quasiparticles. In the absence of SOC, there exists a broad regime of phase separation, where the system enjoys minimizing its free energy through phase separating into the fully paired SF phase and the magnetized normal phase. The effect of SOC is dramatic at zero temperature: The system is unstable to phase separation at any polarization without SOC; however, as the SOC is turned on, the system is a ''magnetized'' superfluid, in which the superfluid component and the normal component coexist in an isotropic and homogeneous fashion. At finite temperature, by increasing the SOC strength λ, both the regions of normal and the phase separation diminishes, leaving the broadened regime of SF_M. The spin-orbit coupling stabilizes the magnetized superfluid phase through mixing of the spin singlet and spin triplet components that supports a finite population

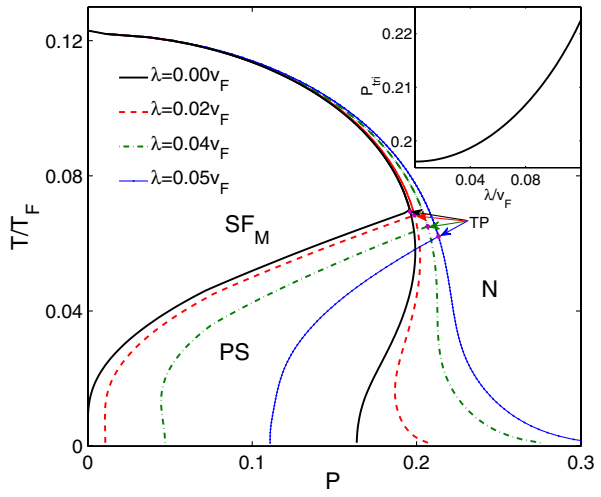

FIG. 3 (color online). Finite-temperature phase diagram in the plane of T and P at $1/k_F a_s = -1$. The inset shows the corresponding polarization P_{tri} for the tricritical point as a function of SOC strength λ. The phase SF is along the line of $P = 0$. The notation is the same as in Fig. 2.

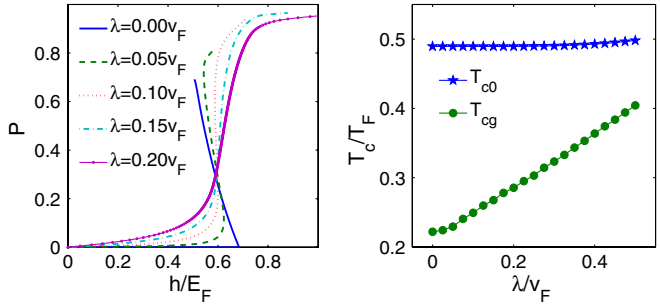

FIG. 4 (color online). Left: The polarization $P = \frac{n_\uparrow - n_\downarrow}{n_\uparrow + n_\downarrow}$ as a function of the magnetic field h for various SOC strength λ at zero temperature at unitarity. Right: The critical temperature for balanced superfluid at unitarity; T_{c0} is calculated from mean-field theory and T_{cg} is calculated by taking account of the Nozieŕes–Schmitt-Rind correction.

imbalance. The tricritical point moves towards high polarization and low temperature when λ is increased, as seen in the inset.

The effect of SOC on the stability of the system manifests itself on the spin susceptibility of the system. We examine the stability of the superfluid phase at unitarity at zero temperature where mean-field theory should give qualitative reasonable arguments. As shown in Fig. 3, at $\lambda = 0$, the system is unstable to phase separation, as the slope of $\delta P/\delta h$ is always either zero or negative. There exists a critical polarization (here $P_c = 0.68$) above which the system reverts to the normal state. When the SOC is turned on, the superfluid state could support both low polarization and high polarization, in contrast to what we saw in Fig. 2 at $1/k_F a_s = -1$, where the superfluid state supports only low polarization. At a sufficient large λ, the slope of the whole curve becomes positive, indicating that it is able to sustain any polarization.

One of the most important questions to ask about the unitary superfluid is how the critical temperature varies with SOC strength. At finite temperature, the contribution from noncondensed pairs to the density $n = \partial\Omega/\partial\mu$ becomes important. This contribution is necessary to approach the transition temperature of an ideal Bose gas in the molecular limit where $T_{\mathrm{BEC}} = 0.218 T_F$ and can be included in the noncondensed phase ($\Delta_0 = 0$) through the Gaussian contribution to the grand potential: $\Omega_g = (1/2\beta V)\sum_{\mathbf{q}, i\nu_m} \ln\Gamma^{-1}(\mathbf{q}, i\nu_m)$, where ν_m denotes the bosonic Matsubara frequencies. For numerical convenience, we treat the fluctuation by adopting the Nozieŕes–Schmitt-Rind scheme [27]. The critical temperature for a balanced superfluid is shown in Fig. 4 at unitarity. The critical temperature calculated from mean-field theory, T_{c0}, starts at a high value and increases slowly at small SOC. By taking account of the Gaussian fluctuation, the critical temperature starts at about $0.224 T_F$ and increases almost linearly with increasing SOC strength λ for low λ, hinting at a possible way of realizing high-T_c superfluids.

Another interesting question concerning two-species spin imbalanced Fermi gases is how the picture of the breached pairing state [19] get modified. Breached pairing is characterized by a phase separation in momentum space between the excess of majority species $\uparrow$ and the minority species $\downarrow$ in the superfluid state. Signatures of phase separation are visible in the momentum distribution $n_{\mathbf{k}\sigma}$ and correlation function $C_{\downarrow\uparrow}(\mathbf{k}) = |\langle \psi_{-\mathbf{k}\downarrow} \psi_{\mathbf{k}\uparrow}\rangle|$. Requiring the pairing amplitude to be zero, one finds the region for phase separation: (i) $k_\perp = 0$ and (ii) $|k_z| \in [0, \sqrt{\mu + \sqrt{h^2 + \Delta_0^2}}]$ if $\mu \le \sqrt{h^2 + \Delta_0^2}$ or $|k_z| \in [\sqrt{\mu - \sqrt{h^2 + \Delta_0^2}}, \sqrt{\mu + \sqrt{h^2 + \Delta_0^2}}]$ if $\mu > \sqrt{h^2 + \Delta_0^2}$. Referring to Fig. 5, for $P = 0.7$ shown in panels (a) and (c), there exists two typical momenta k_{c1} and k_{c2} between which the minority species $\downarrow$ is depleted and the majority species has full occupation, reminiscent of a breached pairing state with two Fermi surfaces (BP_2), while for $P = 0.9$ shown in panels (b) and (d), there exists a typical momentum k_c below which the minority species is depleted and the majority species becomes fully occupied, reminiscent of BP_1. In both cases, the correlation function shows a "hole" for momenta less than the Fermi momentum of the majority quasiparticles. The momentum distribution and the pairing amplitude bear consequences for experimental observation. The single-particle momentum distribution of trapped Fermi gases is routinely observed by time-of-flight measurements [28].

In summary, we have identified a series of new features arising from spin-orbit coupling. We hope that current work will add new excitement to the surging field of cold atom physics involving an artificial gauge field and spin-orbit coupling.

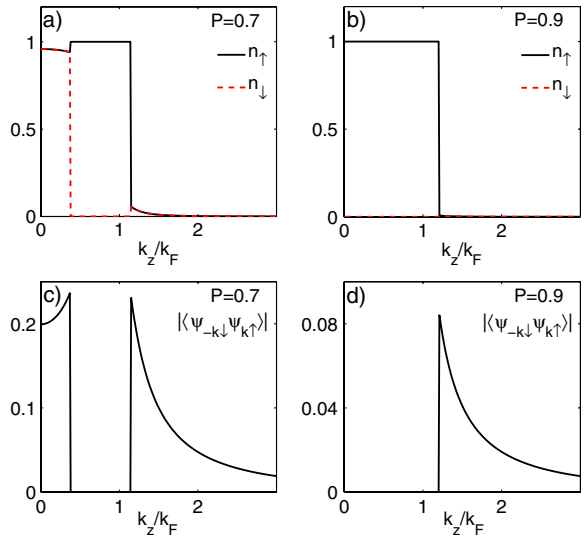

FIG. 5 (color online). The momentum distribution $n_{\mathbf{k}\sigma}$ and correlation function $C_{\downarrow\uparrow}(\mathbf{k}) = |\langle\psi_{-\mathbf{k}\downarrow}\psi_{\mathbf{k}\uparrow}\rangle|$ at unitarity at zero temperature with SO coupling strength $\lambda = 0.2v_F$ for two typical polarizations: $P = 0.7$ (left) and $P = 0.9$ (right).

This work was supported by the NKBRSFC under Grants No. 2011CB921502, No. 2012CB821305, No. 2009CB930701, and No. 2010CB922904, NSFC under Grants No. 10934010 and No. 60978019, and NSFC-RGC under Grants No. 11061160490 and No. 1386-N-HKU748/10.

[1] Y.-J. Lin, R. L. Compton, K. Jiménez-Garcia, J. V. Porto, and I. B. Spielman, Nature (London) **462**, 628 (2009).
[2] Y.-J. Lin, K. Jiménez-Garcia, and I. B. Spielman, Nature (London) **471**, 83 (2011).
[3] D. Xiao, M.-C. Chang, and Q. Niu, Rev. Mod. Phys. **82**, 1959 (2010).
[4] M. Z. Hasan and C. L. Kane, Rev. Mod. Phys. **82**, 3045 (2010).
[5] M. Sato, Y. Takahashi, and S. Fujimoto, Phys. Rev. Lett. **103**, 020401 (2009).
[6] J. D. Sau, R. Sensarma, S. Powell, I. B. Spielman, and S. DasSarma, Phys. Rev. B **83**, 140510 (2011).
[7] J. P. Vyasanakere and V. B. Shenoy, Phys. Rev. B **83**, 094515 (2011).
[8] J. P. Vyasanakere, S. Zhang, and V. B. Shenoy, Phys. Rev. B **84**, 014512 (2011).
[9] Z.-Q. Yu and H. Zhai, Phys. Rev. Lett. **107**, 195305 (2011).
[10] H. Hu, L. Jiang, X.-J. Liu, and H. Pu, Phys. Rev. Lett. **107**, 195304 (2011); L. Jiang, X.-J. Liu, H. Hu, and H. Pu, Phys. Rev. A **84**, 063618 (2011).
[11] M. Gong, S. Tewari, and C. Zhang, Phys. Rev. Lett. **107**, 195303 (2011); G. Chen, M. Gong, and Chuanwei Zhang, Phys. Rev. A **85**, 013601 (2012).
[12] M. Iskin and A. L. Subasi, Phys. Rev. Lett. **107**, 050402 (2011); Phys. Rev. A **84**, 043621 (2011).
[13] K. Seo, L. Han, and C. A. R. S. Melo, arXiv:1106.3613.
[14] W. Yi and G.-C. Guo, Phys. Rev. A **84**, 031608 (2011).
[15] L. P. Gor'kov and E. I. Rashbar, Phys. Rev. Lett. **87**, 037004 (2001).
[16] S. Giorgini, L. P. Pitaevskii, and S. Stringari, Rev. Mod. Phys. **80**, 1215 (2008); G. B. Patridge *et al.*, Science **311**, 503 (2006); M. W. Zwierlein *et al.*, Science **311**, 492 (2006).
[17] P. Fulde and R. A. Ferrell, Phys. Rev. **135**, A550 (1964); A. I. Larkin and Y. N. Ovchinnikov, Sov. Phys. JETP **20**, 762 (1965).
[18] H. Muther and A. Sedrakian, Phys. Rev. Lett. **88**, 252503 (2002).
[19] W. V. Liu and F. Wilczek, Phys. Rev. Lett. **90**, 047002 (2003).
[20] D. E. Sheehy and L. Radzihovsky, Phys. Rev. Lett. **96**, 060401 (2006); C.-H. Pao, S.-T. Wu and S.-K. Yip, Phys. Rev. B **73**, 132506 (2006).
[21] M. M. Parish, F. M. Marchetti, A. Lamacraft, and B. D. Simons, Nature Phys. **3**, 124 (2007).
[22] M. M. Parish, F. M. Marchetti, A. Lamacraft, and B. D. Simons, Phys. Rev. Lett. **98**, 160402 (2007).
[23] J. T. Stewart, J. P. Gaebler, and D. S. Jin, Nature (London) **454**, 744 (2008); J. P. Gaebler *et al.*, Nature Phys. **6**, 569 (2010).
[24] Y. il Shin, C. H. Schunck, A. Schirotzek, and W. Ketterle, Nature (London) **451**, 689 (2008).
[25] G. Sarma, J. Phys. Chem. Solids **24**, 1029 (1963).
[26] R. Casalbuoni and G. Nardulli, Rev. Mod. Phys. **76**, 263 (2004).
[27] P. Nozieŕes and S. Schmitt-Rind, J. Low Temp. Phys. **59**, 195 (1985).
[28] C. A. Regal, M. Greiner, S. Giorgini, M. Holland, and D. S. Jin, Phys. Rev. Lett. **95**, 250404 (2005).